JACS
JOURNAL OF THE AMERICAN CHEMICAL SOCIETY
Article
pubs.acs.org/JACS

Synthesis and Characterization of Thorium(IV) and Uranium(IV) Corrole Complexes

Ashleigh L. Ward,[†] Heather L. Buckley,[†] Wayne W. Lukens,[‡] and John Arnold*[,†]

[†]Department of Chemistry, University of California, Berkeley, California 94720, United States
[‡]Chemical Sciences Division, Lawrence Berkeley National Laboratory, Berkeley, California 94720, United States

Supporting Information

ABSTRACT: The first examples of actinide complexes incorporating corrole ligands are presented. Thorium(IV) and uranium(IV) macrocycles of Mes_2(*p*-OMePh)corrole were synthesized via salt metathesis with the corresponding lithium corrole in remarkably high yields (93% and 83%, respectively). Characterization by single-crystal X-ray diffraction revealed both complexes to be dimeric, having two metal centers bridged via bis(μ-chlorido) linkages. In each case, the corrole ring showed a large distortion from planarity, with the Th(IV) and U(IV) ions residing unusually far (1.403 and 1.330 Å, respectively) from the N_4 plane of the ligand. ^{1}H NMR spectroscopy of both the Th and U dimers revealed dynamic solution behavior. In the case of the diamagnetic thorium corrole, variable-temperature, DOSY (diffusion-ordered) and EXSY (exhange) ^{1}H NMR spectroscopy was employed and supported that this behavior was due to an intrinsic pseudorotational mode of the corrole ring about the M−M axis. Additionally, the electronic structure of the actinide corroles was assessed using UV−vis spectroscopy, cyclic voltammetry, and variable-temperature magnetic susceptibility. This novel class of macrocyclic complexes provides a rich platform in an underdeveloped area for the study of nonaqueous actinide bonding and reactivity.

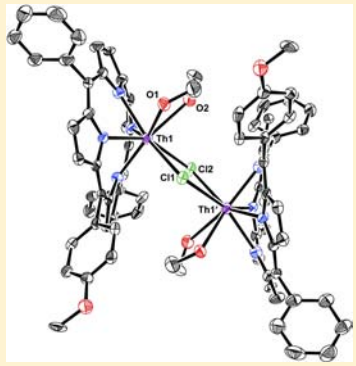

INTRODUCTION

The organometallic and coordination chemistry of actinide elements has become a subject of increasing interest over the past decade.[1−6] Despite this recent surge, the study of nonaqueous actinides remains underexplored when compared to that of the s, p, and d blocks or even lanthanides. A better understanding of the differences in covalency between the 4f and 5f elements, as well as actinide−ligand complex formation, has direct implications for improving nuclear waste remediation schemes.[7,8] Additionally, actinides have access to a wide variety of oxidation states and possess f orbitals capable of participating in bonding, allowing them to offer reactivity modes different from those of their better studied transition-metal and lanthanide counterparts. Recognition of these unique attributes has led to the discovery of actinide coordination compounds that facilitate small molecule activation,[9,10] atom-transfer reactions,[11,12] and hydrocarbon functionalization,[13,14] providing ample motivation for the development of both novel actinide systems and catalytic methodologies.[15,16]

Due in large part to the kinetic and thermodynamic stability afforded via the macrocyclic effect,[17] crown ethers,[18] calixarenes,[19] and more recently "Pacman" polypyrroles[20] have been widely utilized for the study of f-element coordination chemistry and separation science. However, the vast majority of work focuses on macrocyclic complexes of the uranyl cation, with low-valent actinide examples remaining largely absent.[21,22] The few exceptions include the thorium[23] and uranium[24] porphyrins first reported in the 1980s. However, in contrast to the plethora of d-element compounds, the actinide examples comprise a body of only nine structurally characterized (and thus far unreactive) complexes, highlighting the dearth of suitable low-valent starting platforms.[25]

Corroles are close relatives of porphyrins; these tribasic, redox-active, and strongly σ donating macrocycles stabilize metals in a wide variety of oxidation states. Additionally, they present an N_4 ring for metal coordination smaller than that of porphyrins, leading to reactive systems by virtue of the out-of-plane nature of many metal ions, while still offering rigid steric protection along one face of the molecule.[26,27] These systems have shown great promise with many mid-to-late transition metals over a wide variety of areas, including catalysis, photochemical sensing, biomedicine, and alternative energy applications.[28−30] Exploiting these properties, in combination with the special features f-element metals afford, yields a novel starting platform for actinides that holds promise for a plethora of applications, including the facilitation of actinide−actinide bonding, support of formally low-valent Th(II) and U(II/III), single-molecule magnetism, and catalytic methodologies. Here, utilizing the recently reported trilithiocorroles,[31] we discuss the synthesis and characterization of the first actinide corroles, featuring uranium(IV) and thorium(IV).

RESULTS AND DISCUSSION

Synthesis and Structural Properties. The complexes $(Mes_2(p\text{-OMePh})corrole)_2Th_2(\mu\text{-Cl})_2(DME)_2$ (**1**) and

Received: July 15, 2013
Published: September 4, 2013

   dx.doi.org/10.1021/ja407203s | J. Am. Chem. Soc. 2013, 135, 13965−13971

Scheme 1. Synthesis of Thorium(IV) Corrole 1 and Uranium(IV) Corrole 2[a]

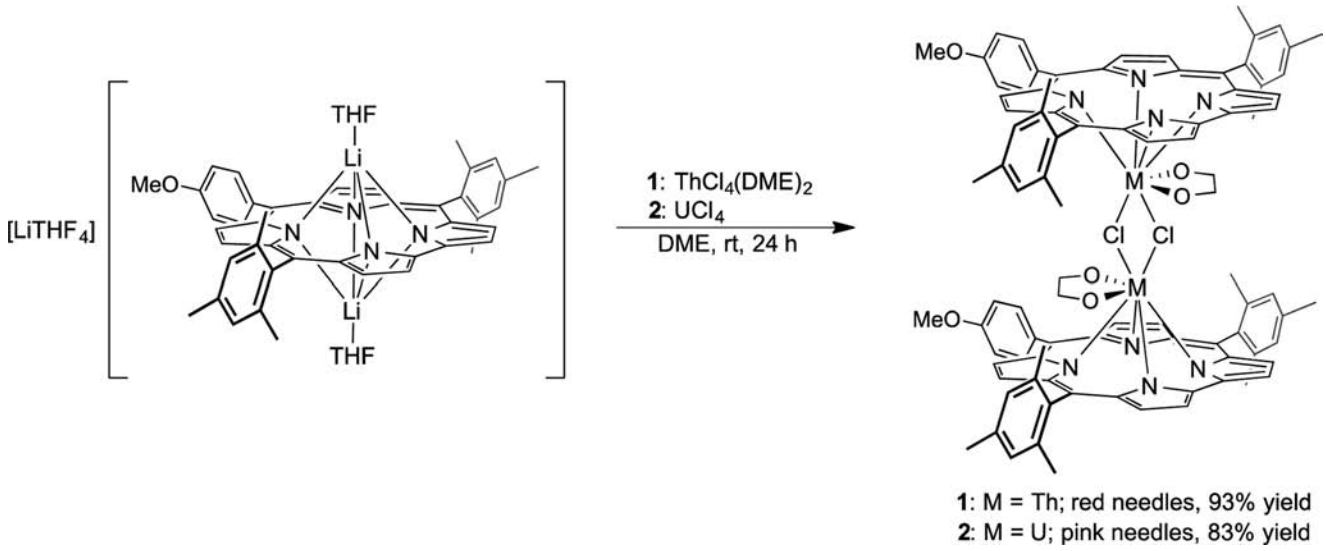

[a]The methyl groups of coordinated DME molecules have been omitted for clarity.

$(Mes_2(p\text{-OMePh})corrole)_2U_2(\mu\text{-Cl})_2(DME)_2$ (**2**) were synthesized via combination in dimethoxyethane (DME) of the corresponding lithium corrole $(Mes_2(p\text{-OMePh})corrole)Li_3\cdot 6THF$[31] with $ThCl_4(DME)_2$[32] and UCl_4,[33] respectively (Scheme 1). Both reactions were stirred at room temperature for 1 d, resulting in precipitation of a purple solid in the case of thorium complex **1**, while a dark red solution was observed for the uranium complex **2**. Evaporation of the solvent under vacuum, followed by recrystallization from a mixture of dichloromethane (DCM) and hexanes, afforded dark red needles of **1** (93% yield) and dark pink needles of **2** (83% yield).

Surprisingly, in comparison to related porphyrin and corrole complexes,[23,24,34] both **1** and **2** crystallize as dimers, with two metal centers joined via bis(μ-chlorido) linkages. This type of structure is unprecedented in corrole chemistry, with the closest examples being the recently reported tungsten and molybdenum μ-oxo compounds,[35,36] and is rare for actinides, particularly with sterically demanding ligands, due to the relatively weak nature of the M−Cl dative bond.[37,38] Thorium(IV) corrole **1** is shown in an ORTEP view in Figure 1; the structure of the U(IV) species is analogous (Figure S7, Supporting Information). Each eight-coordinate metal atom is bound by a trianionic corrole, a bidentate DME ligand, and two chlorides (additional crystallographic details are presented in Table 1). This is in contrast to the recently reported lanthanide corroles, as well as the actinide porphyrins, which are all monomeric.[23,24,34]

The coordination geometry about the metal center is approximately dodecahedral, and both the metal−chloride (Th1−Cl1, 2.932(2) Å; Th1−Cl2, 2.886(1) Å; U1−Cl1, 2.873(2) Å; U1−Cl2, 2.840(1) Å) and metal−solvent (Th1−O1, 2.665(5) Å; Th1−O2, 2.586(5) Å; U1−O1, 2.659(6) Å; U1−O2, 2.555(5) Å) interactions are characteristic of those of other Th(IV) and U(IV) complexes.[32,33,40−43] The Th−Th1′ distance of 4.7279(4) Å and U1−U1′ distance of 4.6621(5) Å are similar to those reported for existing chloride diamond-core Th(IV) and U(IV) compounds.[38,42−45] The average Th−N distance (2.39(1) Å) is longer than is typical for a Th−amido bond, but comparable to that of the thorium(IV) porphyrin (2.40 Å).[23] Likewise, the average U−N distance of 2.33(1) Å is slightly shorter than the analogous uranium(IV) porphyrin U−N distance at 2.41 Å.[24] As is expected given the smaller ionic radius of uranium, this is also slightly shorter than the Th−N corrole distance.

The thorium center in **1** is located 1.403 Å above the N_4 plane (as defined by the nitrogen atoms of the corrole), while the uranium of **2** is displaced by 1.330 Å. In **1**, the metal−plane distance is slightly shorter than that of the thorium porphyrin (1.424 Å). In complex **2**, the opposite is true: the corresponding uranium porphyrin shows a value of 1.29 Å. The larger ring size of the porphyrin, difference in charge on the macrocycle (dianionic vs trianionic), varying coordination

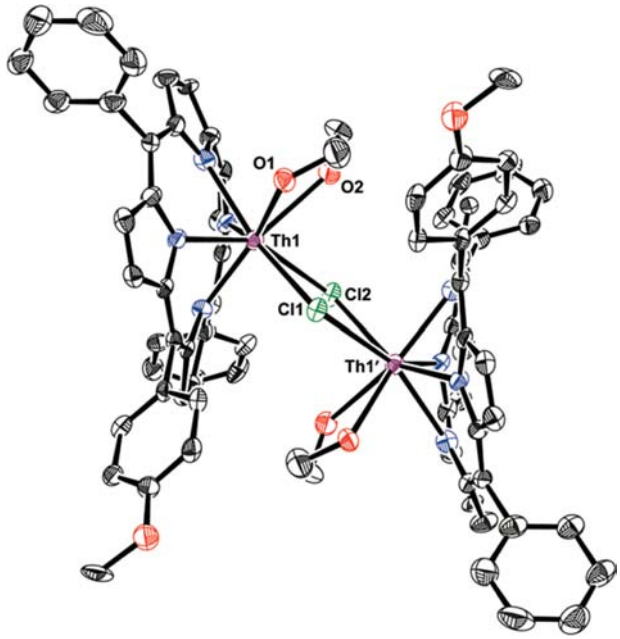

Figure 1. Molecular structure of thorium(IV) corrole **1**. Thermal ellipsoids are set to a 50% probability level. Hydrogen atoms, and both the mesityl and DME methyl groups, have been omitted for clarity.[39]

dx.doi.org/10.1021/ja407203s | J. Am. Chem. Soc. 2013, 135, 13965−13971

Table 1. Crystal and Refinement Data for Complexes 1 and 2

	1	2
formula	$C_{96}H_{94}Cl_2N_8O_6Th_2$	$C_{96}H_{94}Cl_2N_8O_6U_2$
mol wt	1990.77	2002.75
space group	*C*2/*c*	*C*2/*c*
a (Å)	26.5585(9)	27.0738(14)
b (Å)	23.3363(9)	23.6955(12)
c (Å)	20.8898(7)	20.6036(11)
α (deg)	90	90
β (deg)	123.790(2)	123.272(2)
γ (deg)	90	90
V (Å^3)	10760.0(7)	11051.0(10)
Z	4	4
ρ_{calcd} (g/cm^3)	1.229	1.204
F_{000}	3952	3968
μ (mm^{-1})	2.858	3.021
no. of reflns collected	29024	37647
no. of independent reflns	9629	10080
R_{int}	0.0660	0.0582
R1, wR2	0.0474/0.1094	0.0527/0.1450
R1 (all data)	0.0757	0.0833
GOF	0.980	1.038
res peak/hole (e$^-$/Å^3)	3.230/−1.332	3.002/−1.016

number, and dimeric structure of corroles **1** and **2** (in contrast to the monomeric porphyrins) can all be considered as competing factors in determining this metric; nonetheless, the differences are not definitively rationalized on the basis of the data available to date. Apart from one lanthanum corrole complex,[34] where the La−N_4 plane distance is 1.469 Å (and the aforementioned thorium porphyrin), the values of **1** and **2** are the largest metal−N_4 plane displacements for any reported macrocycle, with the next closest being the bismuth corrole distance at 1.15 Å.[46] The fact that thorium and uranium are slightly closer to the corrole than the lanthanum is consistent with the difference in radii, both ionic and covalent, of the metals involved.[47,48]

Absorption Spectroscopy. The two actinide corroles yield nearly identical UV−vis spectra (Figure 2), with each displaying a single Soret band (428 and 427 nm for **1** and **2**, respectively). This peak is markedly different from those observed for both the free-base and lithiated chromophores and is indicative of a loss of planarity of the corrole. Similar spectra are observed for the gallium, zirconium, aluminum, and lanthanide corroles, which all possess significant ring distortion as a result of the metal center sitting significantly above the plane of the ligand.[31,34,49,50] Additionally, both complexes show

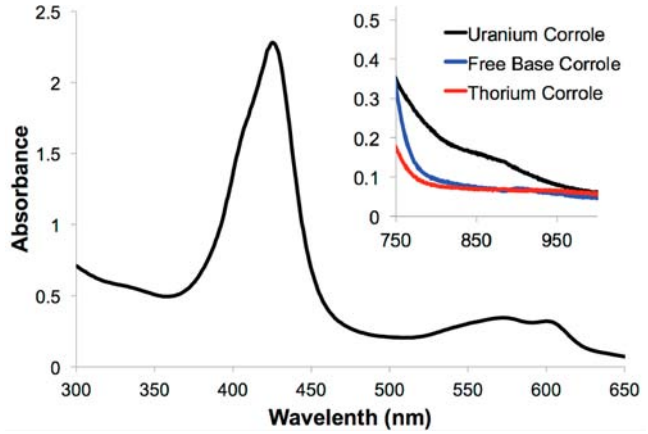

Figure 2. UV−vis absorption spectrum of **2** (1 *μ*M) in DCM. The spectrum for **1** is analogous (see the Supporting Information, Figure S10). Inset: overlay of the absorption spectra of **1**, **2**, and the free-base corrole (10 mM) in DCM.

two broad Q bands, at 576 and 600 nm for **1** and 575 and 602 nm for **2**, respectively, consistent with HOMO and LUMO transitions described by the Gouterman four-orbital model for corroles.[51] At much higher concentrations (10 mM), a band is visible at 880 nm for the uranium complex (Figure 2, inset). This feature is absent from the spectra of both the thorium and free-base corroles and may arise as a result of an increased allowedness of f−f transitions due to coupling across the chloride bridges. However, the large extinction coefficients of corroles, combined with the relatively low intensity of Laporte forbidden f−f transitions, prevent sufficient resolution for definitive assignment.

NMR Spectroscopy. The ambient-temperature ^{1}H NMR spectrum of **1** is straightforward in the aliphatic region. Four singlets can be assigned to the one *p*-methoxy and three mesityl CH_3 protons. Two additional broadened singlets correspond to the protons of the coordinated DME molecule, which exchange rapidly in CD_3CN. However, the resonances in the aromatic region are broadened at room temperature. Upon cooling to −30 °C, the aromatic peaks can be resolved, but additional peaks are observed in the aliphatic region. The dynamic solution behavior seen in the aromatic region is similar to that observed for the analogous lanthanide corroles and is attributed to the highly facile exchange of coordinating solvent.[34] However, the splitting of the aliphatic peaks is unique to the dimeric actinide corroles and therefore could be due either to an equilibrium between the dimer observed in the solid state

Scheme 2. Pseudorotation about the Th−Th Axis of 1, Averaging to a C_{2v} Symmetry at Elevated Temperatures, but Locking into a C_2 Symmetry upon Cooling

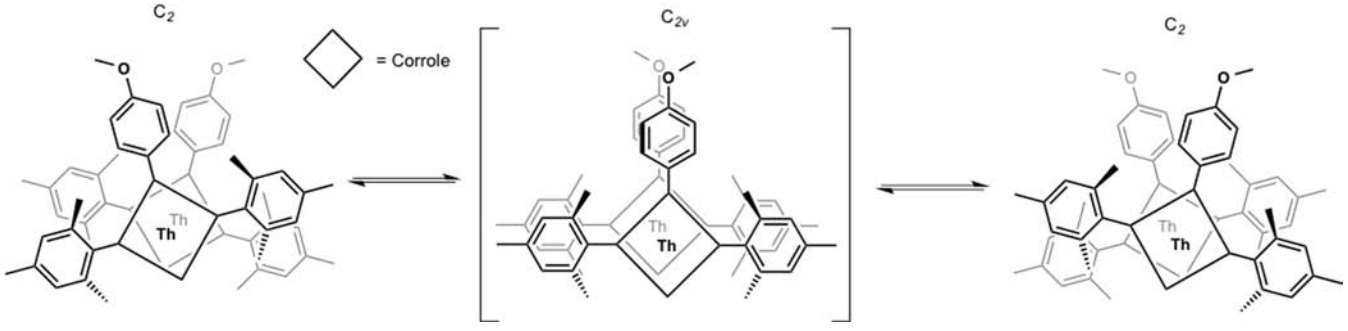

dx.doi.org/10.1021/ja407203s | J. Am. Chem. Soc. 2013, 135, 13965−13971

and a potential monomer in solution or to an intrinsic pseudorotational mode of the dimer complex itself (Scheme 2).

Upon performing DOSY (diffusion-ordered) ^{1}H NMR spectroscopy, a single diffusion coefficient was observed (2.55 $\times$ 10^{-6} cm^2 s^{-1}), consistent with the presence of the dimeric species (r_s = 9.9 Å) (see the Supporting Information, Figure S6). At low temperature, six singlets were observed for the mesityl CH_3 protons, implying two inequivalent sets of mesityl groups, consistent with C_2 symmetry, and mirroring what is observed in the crystal structure. The EXSY (exchange) ^{1}H NMR of **1** at −30 °C (see the Supporting Information, Figure S5) exhibited cross-peaks showing chemical exchange between the two sets of mesityl methyls, implying that the dynamic process was only slowed, and not averted, at this temperature. Upon warming, a rapid pseudorotation along the Th−Th axis leads to an averaging of the chemical environment that results in a C_{2v} symmetry whereby the six mesityl groups are equivalent (Scheme 2). This rotational process is further supported by the behavior of the *p*-methoxy group, which remains equivalent by virtue of a C_2 axis even in the staggered conformation and is thus observed as a single peak across varying temperatures. The proton resonances for **2** are broad and paramagnetically shifted, as expected for a complex with an f^2 uranium(IV) center (see below).

Electrochemistry. Cyclic voltammetry (CV) experiments show that the thorium corrole undergoes two reversible processes ($E_{1/2}$ = 124 and 616 mV; Figure 3). Additionally, there is an irreversible oxidation at 1.32 V and an irreversible reduction at −1.81 V. Thorium(IV) is not expected to display any redox behavior within the potential range discussed here.[52] Therefore, these features may confidently be regarded as ligand-based processes, arising from changes in the macrocycle electronic structure due to both the electron-withdrawing effect of the metal center and the extreme distortion of the corrole ring from planarity upon binding to the actinide. This effect has been observed for a variety of non-redox-active metals upon corrole chelation, where, generally, the redox potential of the metallocorrole correlates well with the electronegativity of the bound ion, as with the P, Al, Ge, Ga, and Sn examples.[49,50,53,54] However, outliers to this trend occur, where Bi, despite being the most electronegative of the aforementioned series, displays the lowest oxidation potential.[46] This electrochemical behavior can be reasonably explained when considering the greater distortion from planarity—and thus aromaticity—seen upon complexation and illustrates the synergy of these two effects.

The cyclic voltammogram for **2** is more complex (Figure 4). The first two oxidations, which were reversible in complex **1**, are only quasireversible ($E_{1/2}$ = 124 and 616 mV) and have additional oxidative shoulders (E_{pa} = 0.44 and 1.05 V). The potential of these shoulders remains constant as a function of the scan rate (Figure 4, inset), eliminating the possibility of an electron transfer−chemical reaction−electron transfer (ECE) mechanism. Additionally, these peaks are absent in the thorium case, indicating that this redox behavior may arise due to electronic communication between the uranium centers, consistent with the low-intensity transition observed in the UV−vis spectrum.[55,56] The oxidations are positively shifted for **2** when compared to **1** (Figure 5), reflecting the larger electronegativity of uranium, as well as the greater distortion of the corrole ring. Additionally, an irreversible oxidation at 1.54 V and a reduction at −1.85 V mirror those seen in the thorium case. The similarity in redox properties between the uranium(IV) and thorium(IV) corroles has also been noted between

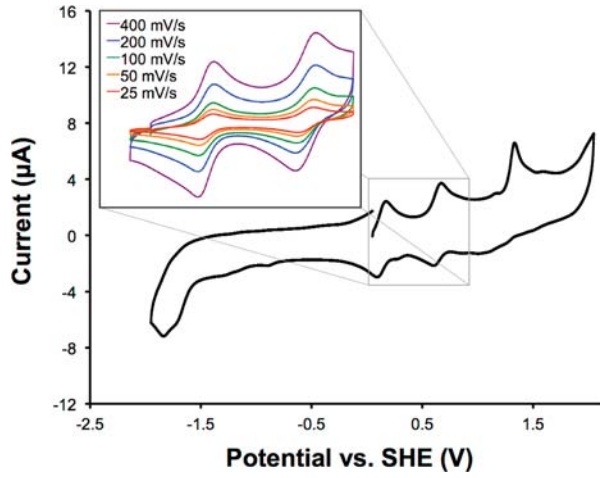

Figure 3. Cyclic voltammagram of **1** (1 mM) at 100 mV/s in MeCN, 25 °C. Inset: variable scan rate cyclic voltammagrams of **1** for the highlighted redox waves.

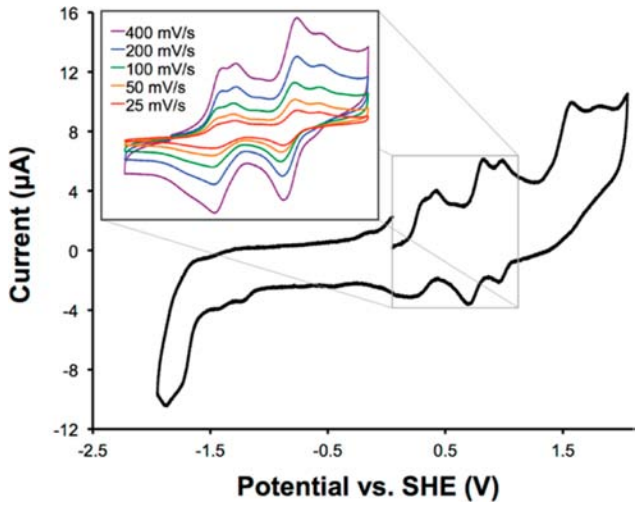

Figure 4. Cyclic voltammagram of **2** (1 mM) at 100 mV/s in MeCN, 25 °C. Inset: Variable scan rate cyclic voltammagrams of **2** for the highlighted redox waves.

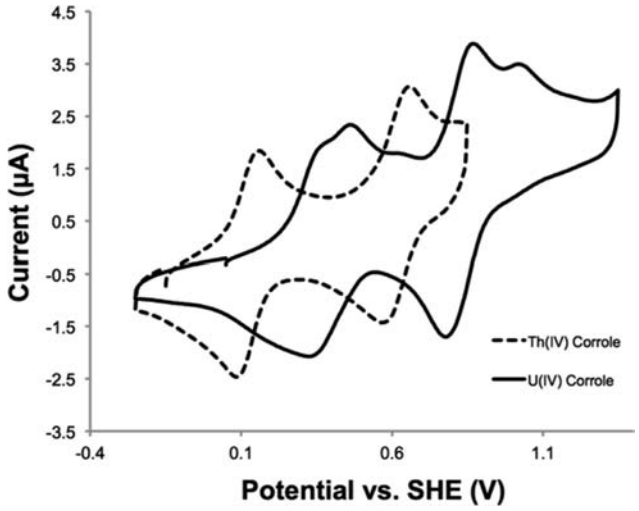

Figure 5. Overlay of cyclic voltammagrams of **1** and **2** (1 mM) at 100 mV/s in MeCN, 25 °C.

dx.doi.org/10.1021/ja407203s | J. Am. Chem. Soc. 2013, 135, 13965−13971

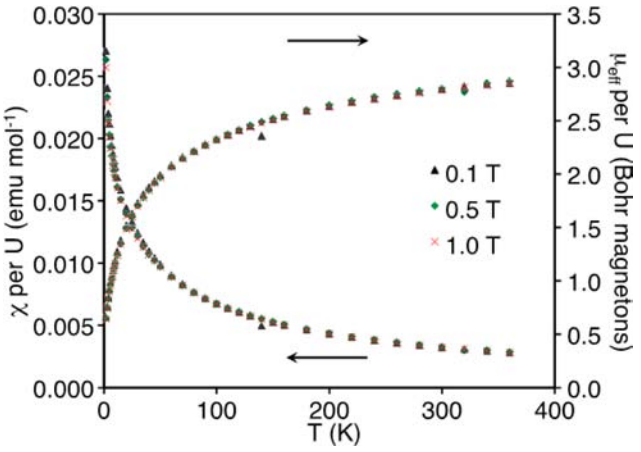

Figure 6. Variable-temperature magnetic susceptibility of **2**.

the actinide porphyrins and is attributed to the ligand-centered nature of the redox processes.[57]

Magnetism. The variable-temperature magnetic moments measured for **2** are in good agreement with those predicted for U(IV) with a $^3H_4$ ground state. Upon cooling, the magnetic moment trends toward zero (Figure 6), consistent with an orbital singlet ground state (m_J = 0) and similar to that observed for related uranium complexes.[58] Likewise, the magnetic moment of **2** at 360 K (2.85 μ_B) is within the range observed for uranium(IV) amide complexes (2.44−3.48 μ_B)[59,60] and similar to that of U(phthalocyanine)$_2$ (ca. 3.1 μ_B).[61] Taken together, these observations lead to the assignment of both metal centers as U(IV).

■ CONCLUSIONS

To summarize, we have prepared and characterized the first examples of actinide corroles in a facile and high-yielding manner. They represent a new class of macrocyclic complexes in an area that is underdeveloped for this group of elements. We believe these compounds have the potential to provide a robust platform for elucidating actinide bonding and reactivity; studies aimed at exploiting this concept are in progress.

■ EXPERIMENTAL SECTION

General Procedures. Unless otherwise noted, all reactions were performed using standard Schlenk line techniques or in an MBraun N_2 atmosphere glovebox (<1 ppm O_2/H_2O). All glassware and Celite were stored in an oven at ca. 150 °C. Dimethoxyethane (DME), acetonitrile (MeCN), tetrahydrofuran (THF), hexane, and dichloromethane (DCM) were dried and degassed using a Phoenix solvent drying system commercially available from JC Meyer Solvent Systems. CD_3CN was vacuum-transferred from CaH_2 and degassed with three freeze−pump−thaw cycles. All NMR spectra were recorded at the specified temperature on Bruker DRX 500 and AV-600 spectrometers. Temperature calibration was performed using changes in chemical shift separation of ethylene glycol at high temperature and methanol at low temperature. ^{1}H chemical shifts (δ) were calibrated using residual solvent peaks. UV−vis spectra were determined with a Varian Cary 50 UV−vis spectrophotometer using a Schlenk-adapted 1 mm quartz cell. Mass spectral data (ESI-MS, positive mode) were obtained at the University of California, Berkeley, Microanalytical Facility using vacuum-dried samples dissolved in THF. Melting points were determined on an Optmelt SRS using sealed capillaries prepared under nitrogen and are uncorrected. (Mes$_2$(*p*-OMePh)corrole)Li$_3$·6THF,[31] $ThCl_4(DME)_2$,[32] and UCl_4[33] were prepared according to literature procedures.

Thorium(IV) 5,15-Bis(2,4,6-trimethylphenyl)-10-(4-methoxyphenyl)corrole Bis(dimethoxyethane) (1). A solution of (Mes$_2$(*p*-OMePh)corrole)Li$_3$·6THF (100 mg, 0.091 mmol) in 2 mL of DME was added to a suspension of $ThCl_4(DME)_2$ (51 mg, 0.092 mmol) in 2 mL of DME to produce a dark red solution. The reaction mixture was stirred for 1 d, after which time a purple solid had precipitated. The reaction mixture was filtered, and the solid was extracted with DCM (2 × 3 mL), filtered through Celite, concentrated until saturation, and carefully layered with hexanes to afford the product as dark red needles (85 mg, 93% yield). Single crystals suitable for X-ray diffraction were obtained by slow evaporation of a solution of **1** in DCM at −40 °C. ^{1}H NMR (500 MHz, CD_3CN, room temperature; note that some peaks are broadened or partially coalesced at this temperature; any assignments were confirmed by spectra taken at additional temperatures): δ 8.07 (s, br, Ar-*H*), 7.32 (s, br, Ar-*H*), 4.04 (s, 3H, $C_6H_4OCH_3$), 3.41 (s, 8H, $(CH_2)_2O_2(CH_3)_2$), 3.25 (s, 12H, $(CH_2)_2O_2(CH_3)_2$), 2.86 (s, 6H, $C_6H_2CH_3$), 2.59 (s, 6H, $C_6H_2CH_3$), 0.91 (s, 6H, $C_6H_2CH_3$). ^{1}H NMR (500 MHz, CD_3CN, −40 °C): δ 8.48 (s, Ar-*H*), 8.44 (s, Ar-*H*), 8.05 (s, Ar-*H*), 7.98 (d, *J* = 10 Hz, Ar-*H*), 7.92 (s, Ar-*H*), 7.72 (s, Ar-*H*), 7.53 (s, Ar-*H*), 7.41 (s, Ar-*H*), 7.30 (s, Ar-*H*), 7.22 (d, *J* = 5 Hz, Ar-*H*), 7.11 (s, Ar-*H*), 6.95 (s, Ar-*H*), 3.96 (s, br), 3.30 (s, br), 3.16 (s, br), 2.92 (s, br), 2.55 (s, br), 2.52 (s, br), 1.84 (s, br), 0.92 (s, br), 0.47 (s, br). UV−vis (nm): 428, 576, 600. ESI-MS (+): *m*/*z* calcd for $C_{48}H_{47}O_3N_4Cl_1Th_1$ 994.3712, obsd 994.3716. Mp: >270.2 °C dec.

Uranium(IV) 5,15-Bis(2,4,6-trimethylphenyl)-10-(4-methoxyphenyl)corrole Bis(dimethoxyethane) (2). A solution of (Mes$_2$(*p*-OMePh)corrole)Li$_3$·6THF (100 mg, 0.091 mmol) in 2 mL of DME was added to a suspension of UCl_4 (35 mg, 0.092 mmol) in 2 mL of DME to produce a dark red solution. The reaction mixture was stirred for 1 d. The solvent was removed in vacuo to yield a dark purple solid. The solid was extracted with DCM (2 × 3 mL), filtered through Celite, concentrated until saturation, and carefully layered with hexanes to afford the product as dark pink needles (76 mg, 83% yield). Single crystals suitable for X-ray diffraction were obtained by slow diffusion of hexane into a solution of **2** in DCM at −40 °C. ^{1}H NMR (500 MHz, CD_3CN, room temperature): δ 10.76 (s, br), 10.28 (s, br), 8.97 (s, br), 8.44 (s, br), 8.37 (s, br), 8.21 (s, br), 8.04 (d, *J* = 5 Hz), 7.49 (s, br), 7.36 (d, *J* = 10 Hz), 7.34 (s, br), 6.66 (s, br), 6.28 (s, br), 5.51 (s, br), 4.13 (s, br), 2.80 (s, br), 2.60 (s, br), 2.35 (s, br), 2.10 (s, br), 3.75−2.00 (s, br, under-reported singlets), 1.90 (s, br), 1.30 (s, br), −8.28 (s, br). ^{1}H NMR (500 MHz, CD_3CN, −40 °C): δ 13.20 (s, br), 10.31 (s, br), 9.21 (s, br), 8.63 (s, br), 8.34 (s, br), 7.57 (s, br), 7.35 (s, br), 7.30 (s, br), 5.59 (s, br), 5.55 (s, br), 4.43 (s, br), 3.39 (s, br), 3.30 (s, br), 3.18 (s, br), 2.56 (s, br), 2.20 (s, br), 1.81 (s, br), 1.24 (s, br), 0.87 (s, br), −1.16 (s, br), −3.24 (s, br), −13.94 (s, br). UV−vis (nm): 427, 575, 602. ESI-MS (+): *m*/*z* calcd for $C_{48}H_{47}O_3N_4Cl_1U_1$ 1000.3839 obsd 1000.3849. Mp: >230.4 °C dec. μ_{eff} = 2.85 μ_B.

Crystallographic Procedures. X-ray structural determinations were performed at CHEXRAY, University of California, Berkeley, on a Bruker APEX II Quazar diffractometer. The instrument is Kappa Geometry with DX and is a three-circle diffractometer that couples a charge-coupled device (CCD) detector[62] with a sealed-tube source of monochromatized Mo Kα radiation. A crystal of appropriate size was coated in Paratone-N oil and mounted on a Kaptan loop. The loop was transferred to the diffractometer, centered in the beam, and cooled by a nitrogen flow low-temperature apparatus that had been previously calibrated by a thermocouple placed at the same position as the crystal. Preliminary orientation matrices and cell constants were determined by collection of 60 10 s frames, followed by spot integration and least-squares refinement. The reported cell dimensions were calculated from all reflections with $I > 10\sigma$. The data were corrected for Lorentz and polarization effects; no correction for crystal decay was applied. An empirical absorption correction based on comparison of redundant and equivalent reflections was applied using SADABS.[63] All software used for diffraction data processing and crystal-structure solution and refinement are contained in the APEX2 program suite (Bruker AXS, Madison, WI).[64] Thermal parameters for all non-hydrogen atoms were refined anisotropically. For all structures, R1 = $\sum(|F_o| - |F_c|)/\sum(|F_o|)$

and wR2 = $[\sum\{w(F_o^2 - F_c^2)^2\}/\sum\{w(F_o^2)^2\}]^{1/2}$, and ORTEP diagrams were created using the ORTEP-3 software package and POV-ray.[65,66]

DOSY NMR Procedure. ^{1}H NMR spectra were recorded on a Bruker AV-600 spectrometer. DOSY spectra were recorded using Bruker's "ledbpgp2s" program with a diffusion delay (D) of 0.08 s and gradient length (δ) of 1300 μs for each sample. T_1 and the 90° pulse width were independently measured prior to the DOSY experiment being run, and the spectra were recorded with a delay of 10 s (4× greater than T_1) to allow for adequate magnetic relaxation. The gradient strength was varied from 5% to 95%. The data were processed using the MestrReNova software package (version 8.1.1).

The hydrodynamic radius of **1** was calculated using the Stokes–Einstein equation:

$$r_s = \frac{KT}{6\pi\eta D}$$

where k is the Boltzmann constant, T is the temperature, η is the viscosity of the liquid, D is the diffusion constant, and r_s is the hydrodynamic radius of the molecule.

Electrochemical Procedures. Solution cyclic voltammograms were recorded with a Gamry Reference 600 potentiostat using a glassy carbon working electrode (0.07 cm^2), a platinum counter electrode, and a floating silver reference electrode. Ferrocene ($E_{Fc}^{+/0}$ = 0.64 V vs SHE) was added at the end of each electrochemical experiment as an internal reference. Acetonitrile was used as the solvent with 0.1 M (^{n}Bu$_4$N)(PF$_6$) as the supporting electrolyte. All examinations of solutions by CV were conducted in an MBraun N_2 atmosphere glovebox (<1 ppm O_2/H_2O).

Magnetism Procedures. Uranium corrole **2** (16.4 mg) was sandwiched between two plugs of quartz wool (Hereaus, 9.9 mg) in a 3 mm o.d. quartz tube, which was flame-sealed on both ends. Sample magnetization was recorded at 0.1, 0.5, and 1 T using a Quantum Designs MPMS SQUID magnetometer. Magnetization was corrected for the diamagnetism of the quartz wool using Pascal's constants (no correction for the diamagnetism of the quartz tube is needed as the quartz tube never leaves the SQUID coils). Molar susceptibility was corrected for the presence of a small amount of ferromagnetic impurity (M_{ferro}) and the diamagnetism of the quart wool (χ_{QW}) and ligands and uranium (χ_{dia}) using Pascal's constants and calculated using the following equation:

$$\chi_{mol} = \frac{\text{moleculer weight}}{\text{sample mass}}\left[\frac{M_{meas} - M_{ferro}}{H} - \chi_{QW}\right] - \chi_{dia}$$

where χ_{mol} is the molar susceptibility, M_{meas} is the measured magnetization, M_{ferro} is the magnetization of the ferromagnetic impurity, which is temperature-independent and assumed to be identical at all fields, χ_{QW} is the contribution to the susceptibility due to the quartz wool, χ_{dia} is the diamagnetic correction, and H is the applied field.

Correction for paramagnetic impurities: Two ferromagnetic impurities are commonly encountered in laboratory samples, steel or iron metal and magnetite or other ferrites from oxide coating on stainless steel laboratory equipment. Of these, magnetite is far more likely to be encountered. In general, the magnetization of ferromagnets is temperature-independent below the Curie temperature, which is 1040 and 860 K for iron and magnetite, respectively, so magnetization of the impurity is temperature-independent for this experiment. The magnetization of ferromagnets is also largely field-independent above the anisotropy field, which is 0.6–1.5 and 0.2 T for steel/iron and magnetite, respectively. Below the anisotropy field, the magnetization of a magnet is roughly linear with the applied field. On the basis of the assumption that the impurity is magnetite or some other ferrite resulting from the abrasion of stainless steel laboratory equipment, the data were corrected for a temperature- and field-independent ferromagnetic impurity. M_{ferro} was allowed to vary to minimize the least-squares difference between χ_{mol} at different fields, which produced a saturation magnetization of M_{ferro} = 1.52 × 10^{-5} emu. Data before and after correction for the presence of the ferromagnetic impurity are shown in Figures S8 and S9 (Supporting Information).

■ ASSOCIATED CONTENT

Supporting Information

Crystallographic data for complexes **1** and **2** (CIF), additional ^{1}H NMR, absorption, and emission spectra, and magnetic susceptibility data. This material is available free of charge via the Internet at http://pubs.acs.org.

■ AUTHOR INFORMATION

Corresponding Author

arnold@berkeley.edu

Notes

The authors declare no competing financial interest.

■ ACKNOWLEDGMENTS

A.L.W. acknowledges the NSF for a GFRP fellowship. H.L.B. acknowledges the International Fulbright Science & Technology Fellowship for support. We are grateful to Antonio DiPasquale (XRD), Thomas Gianetti (NMR), Andy Nguyen (CV), and Zhongrui Zhou (MS) for assistance with instrumentation, as well as Prof. Daniel Gryko and Drs. Casey Brown and Greg Nocton for helpful discussions. This work was supported by the U.S. Department of Energy, Basic Energy Sciences, Chemical Sciences, Biosciences, and Geosciences Division, and a portion was performed at Lawrence Berkeley National Laboratory under Contract No. DE-AC02-05CH11231.

■ REFERENCES

(1) Jones, M. B.; Gaunt, A. J. *Chem. Rev.* **2013**, *113*, 1137.
(2) Liddle, S. T.; Mills, D. P. *Dalton Trans.* **2009**, 5592.
(3) Edelmann, F. T. *Coord. Chem. Rev.* **2012**, *256*, 1151.
(4) Ephritikhine, M. *Dalton Trans.* **2006**, 2501.
(5) Sessler, J. L.; Melfi, P. J.; Pantos, G. D. *Coord. Chem. Rev.* **2006**, *250*, 816.
(6) Bart, S. C.; Meyer, K. In *Structure and Bonding (Berlin, Germany)*; Albrecht-Schmitt, T. E., Ed.; Springer: Berlin, 2008; Vol. *127*.
(7) International Atomic Energy Agency. *Spent Fuel Reprocessing Options*; Vienna, Austria, 2009.
(8) *Nuclear Energy Advisory Committee Report*; U.S. Department of Energy: Washington, DC, 2008.
(9) Cloke, F. G. N.; Hitchcock, P. B. *J. Am. Chem. Soc.* **2002**, *124*, 9352.
(10) Castro-Rodriguez, I. *Science* **2004**, *305*, 1757.
(11) Evans, W. J. *Science* **2005**, *309*, 1835.
(12) Peters, R. G.; Warner, B. P.; Burns, C. J. *J. Am. Chem. Soc.* **1999**, *121*, 5585.
(13) Pool, J. A.; Scott, B. L.; Kiplinger, J. L. *J. Am. Chem. Soc.* **2005**, *127*, 1338.
(14) Barnea, E.; Eisen, M. *Coord. Chem. Rev.* **2006**, *250*, 855.
(15) Andrea, T.; Eisen, M. S. *Chem. Soc. Rev.* **2008**, *37*, 550.
(16) Fox, A. R.; Bart, S. C.; Meyer, K.; Cummins, C. C. *Nature* **2008**, *455*, 341.
(17) Cabbiness, D. K.; Margerum, D. W. *J. Am. Chem. Soc.* **1969**, *91*, 6540.
(18) Clark, D. L.; Keogh, D. W.; Palmer, P. D.; Scott, B. L.; Tait, C. D. *Angew. Chem., Int. Ed.* **1998**, *37*, 164.
(19) Beer, P. D.; Drew, M. G. B.; Hesek, D.; Kan, M.; Nicholson, G.; Schmitt, P.; Sheen, P. D.; Williams, G. *J. Chem. Soc., Dalton Trans.* **1998**, 2783.
(20) Arnold, P. L.; Patel, D.; Wilson, C.; Love, J. B. *Nature* **2008**, *451*, 315.
(21) Alexander, V. *Chem. Rev.* **1995**, *95*, 273.
(22) Sessler, J. L.; Vivian, A. E.; Seidel, D.; Burrell, A. K.; Hoehner, M.; Mody, T. D.; Gebauer, A.; Weghorn, S. J.; Lynch, V. *Coord. Chem. Rev.* **2001**, *216*, 411.

(23) Dormond, A.; Belkalem, B.; Charpin, P.; Lance, M.; Vigner, D.; Folcher, G.; Guilard, R. *Inorg. Chem.* **1986**, *25*, 4785.
(24) Girolami, G. S.; Milam, S. N.; Suslick, K. S. *Inorg. Chem.* **1987**, *26*, 343.
(25) Based on a search of the Cambridge Structural Database. The latest update to the database at the time of writing was February 2013.
(26) Aviv, I.; Gross, Z. *Chem. Commun.* **2007**, *20*, 1987.
(27) Aviv-Harel, I.; Gross, Z. *Chem.—Eur. J.* **2009**, *15*, 8382.
(28) Palmer, J. H. *Structure and Bonding (Berlin, Germany)*; Springer: Berlin, 2011; Vol. *142*, p 49.
(29) Gross, Z. *J. Biol. Inorg. Chem.* **2001**, *6*, 733.
(30) Aviv-Harel, I.; Gross, Z. *Coord. Chem. Rev.* **2010**, *7*, 1.
(31) Buckley, H. L.; Chomitz, W. A.; Koszarna, B.; Tasior, M.; Gryko, D. T.; Brothers, P. J.; Arnold, J. *Chem. Commun.* **2012**, *48*, 10766.
(32) Cantat, T.; Scott, B. L.; Kiplinger, J. L. *Chem. Commun.* **2010**, *46*, 919.
(33) Kiplinger, J. L.; Morris, D. E.; Scott, B. L.; Burns, C. J. *Organometallics* **2002**, *21*, 5978.
(34) Buckley, H. L.; Anstey, M. R.; Gryko, D. T.; Arnold, J. *Chem. Commun.* **2013**, *49*, 3104.
(35) Nigel-Etinger, I.; Goldberg, I.; Gross, Z. *Inorg. Chem.* **2012**, *51*, 1983.
(36) Nigel-Etinger, I.; Goldberg, I.; Gross, Z. *Inorg. Chem.* **2013**, *52*, 4139.
(37) Evans, W. J.; Nyce, G. W.; Greci, M. A.; Ziller, J. W. *Inorg. Chem.* **2001**, *40*, 6725.
(38) Jantunen, K. C.; Batchelor, R. J.; Leznoff, D. B. *Organometallics* **2004**, *23*, 2186.
(39) In the solid state, each dimer possesses an inversion center located between the chlorides, making the two halves of the molecule crystallographically equivalent. As such, the metal centers in Figure 1 and Figure S7 in the Supporting Information are labeled M and M′, respectively.
(40) Liddle, S. T.; Mcmaster, J.; Mills, D. P.; Blake, A. J.; Jones, C.; Woodul, W. D. *Angew. Chem., Int. Ed.* **2009**, *48*, 1077.
(41) McCullough, L. G.; Turner, H. W.; Andersen, R. A.; Zalkin, A.; Templeton, D. H. *Inorg. Chem.* **1981**, *20*, 2869.
(42) Stubbert, B. D.; Marks, T. J. *J. Am. Chem. Soc.* **2007**, *129*, 6149.
(43) Patel, D.; Moro, F.; Mcmaster, J.; Lewis, W.; Blake, A. J.; Liddle, S. T. *Angew. Chem., Int. Ed.* **2011**, *50*, 10388.
(44) Jantunen, K. C.; Haftbaradaran, F.; Katz, M. J.; Batchelor, R. J.; Schatte, G.; Leznoff, D. B. *Dalton Trans.* **2005**, *18*, 3083.
(45) Mills, D. P.; Moro, F.; McMaster, J.; van Slageren, J.; Lewis, W.; Blake, A. J.; Liddle, S. T. *Nat. Chem.* **2011**, *3*, 454.
(46) Reith, L. M.; Stiftinger, M.; Monkowius, U.; Knör, G.; Schoefberger, W. *Inorg. Chem.* **2011**, *50*, 6788.
(47) Shannon, R. D. *Acta Crystallogr., A* **1976**, *32*, 751.
(48) Pyykkö, P.; Atsumi, M. *Chem.—Eur. J.* **2009**, *15*, 186.
(49) Vestfrid, J.; Botoshansky, M.; Palmer, J. H.; Durrell, A. C.; Gray, H. B.; Gross, Z. *J. Am. Chem. Soc.* **2011**, *133*, 12899.
(50) Bendix, J.; Dmochowski, I.; Gray, H.; Mahammed, A.; Simkhovich, L.; Gross, Z. *Angew. Chem., Int. Ed.* **2000**, *39*, 4048.
(51) Ghosh, A.; Wondimagegn, T.; Parusel, A. B. J. *J. Am. Chem. Soc.* **2000**, *122*, 5100.
(52) Stoll, M. E. In *Encyclopedia of Electrochemistry*; Bard, A. J., Ed.; Wiley-VCH: New York, 2007; Vol. *8*.
(53) Aviv-Harel, I.; Gross, Z. *Coord. Chem. Rev.* **2011**, *255*, 717.
(54) Simkhovich, L.; Mahammed, A.; Goldberg, I.; Gross, Z. *Chem.—Eur. J.* **2001**, *7*, 1041.
(55) Evans, K. *Coord. Chem. Rev.* **2006**, *250*, 25.
(56) Palmer, J. H.; Mahammed, A.; Lancaster, K. M.; Gross, Z.; Gray, H. B. *Inorg. Chem.* **2009**, *48*, 9308.
(57) Kadish, K. M.; Moninot, G.; Hu, Y.; Dubois, D.; Ibnlfassi, A.; Barbe, J. M.; Guilard, R. *J. Am. Chem. Soc.* **1993**, *115*, 8153.
(58) Edelstein, N. M.; Lander, G. H. In *The Chemistry of the Actinide and Transactinide Elements*; Morss, L. R., Edelstein, N. M., Fuger, J., Eds.; Springer: Dordrecht, The Netherlands, 2006; Vol. *4*.
(59) Stewart, J. L.; Andersen, R. A. *New J. Chem.* **1995**, *19*, 587.
(60) Reynolds, J. G.; Zalkin, A.; Templeton, D. H.; Edelstein, N. M. *Inorg. Chem.* **1977**, *16*, 599.
(61) Lux, F.; Dempf, D.; Graw, D. *Angew. Chem., Int. Ed. Engl.* **1968**, *7*, 819.
(62) *SMART: Area Detector Software Package*; Bruker Analytical X-ray Systems Inc.: Madison WI, 2003.
(63) *SADABS: Bruker-Nonius Area Detector Scaling and Absorption*, V2.05; Bruker Analytical X-ray Systems Inc.: Madison, WI, 2003.
(64) Sheldrick, G. M. *Acta Crystallogr., A* **2008**, *64*, 112.
(65) Farrugia, L. J. *Appl. Crystallogr.* **1997**, *30*, 565.
(66) van der Sluis, P.; Spek, A. L. *Acta Crystallogr., A* **1990**, *46*, 194.